ALLEN INSTITUTE for BRAIN SCIENCE
Fueling Discovery

TECHNICAL WHITE PAPER:
BIOPHYSICAL MODELING - PERISOMATIC

OVERVIEW

The experimental data collected as part of the Allen Cell Types Database are necessary to the development of an integrated framework for understanding the components of the mouse visual cortex. To continue toward that goal, biophysically detailed models of single neurons recorded *in vitro* have also been created (**Figure 1**). These models have been built from matching electrophysiological and morphological data collected from individual neurons.

These models characterize the firing properties of different cell types in the mouse visual cortex and relate them to generalized biophysical mechanisms governing this firing. Biophysically detailed models may also generalize to different types of input more naturally than more abstract models. The models presented in the database differ from other collections of models in that they are built from data obtained in a highly standardized way and are presented alongside the original experimental data upon which they are based. These models can be downloaded by users for their own modeling studies, and they can also serve as building blocks for larger biophysically-detailed network models. For this latter purpose, an additional advantage of these models is that they include information about the identity of the originally modeled neuron through Cre-based labeling and their location within the cortex. These labels can serve as a link to other experimental modalities.

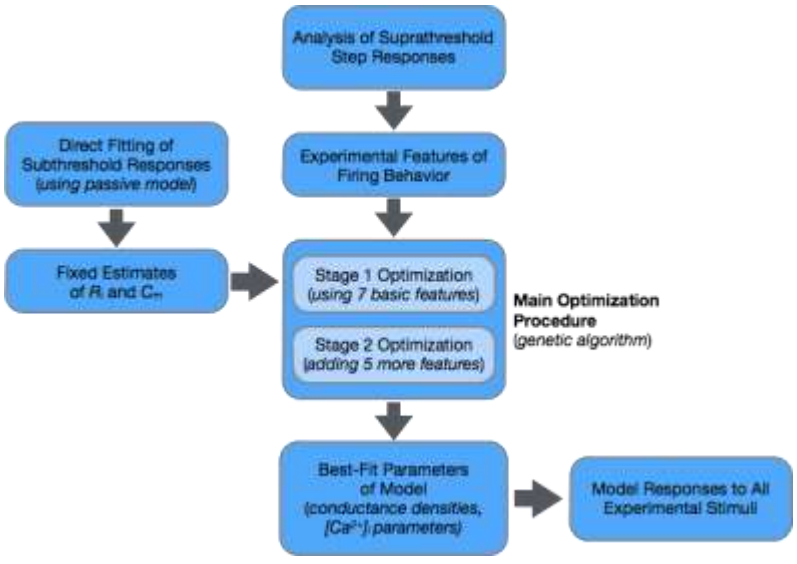

Figure 1. Summary of the generation of biophysical models.
Schematic illustrating the different steps and types of information used to construct biophysical models. The main optimization procedure used a genetic algorithm method to best match features of the neuron's firing behavior as evoked by a step current stimulus.

FEATURE ANALYSIS

The aim in developing these biophysical models was to reproduce the general firing and subthreshold dynamics of the original experimentally-recorded neurons. Models were developed for individual cells: each model has been optimized to match the electrophysiological characteristics of a particular recorded cell. The approach of Druckmann *et al*. (2007) was used to evaluate a model's performance by comparing the model and experimental values of specific electrophysiological features computed from the somatic voltage response to somatic current injection. Earlier studies suggested that using feature comparison can be more robust than matching the experimental voltage trace directly (Druckmann *et al*., 2007), as it allows intrinsic biological variability to be incorporated directly (versus choosing a single trace for comparison) and avoids the unbalanced weighting that can result from action potentials (a major feature of interest) being represented by relatively few points of the voltage trace due to their rapid time course.

The biophysically detailed models were optimized on experimental responses to current steps at the cell body (**Figure 2**), as previous work (Druckmann *et al*., 2011) indicated that models trained on steps generalize better to other stimulus types than models trained on ramp or noise stimuli. A set of 12 features was computed from the somatic membrane voltage traces (**Table 1**, see also Electrophysiology whitepaper in Documentation for the definitions and illustrations of the features). These features were averaged across repeats of the same stimulus protocol applied to the recorded cell, and the experimental variability (standard deviation) of each feature was also recorded. Before feature analysis, experimental traces were corrected for a –14 mV junction potential (*i.e.* the junction potential was added to the experimental trace to get the actual membrane voltage; see also Electrophysiology whitepaper in Documentation for measurement of the junction potential). After models were run, the junction potential was subtracted from the model traces for comparison with the original electrophysiological recordings.

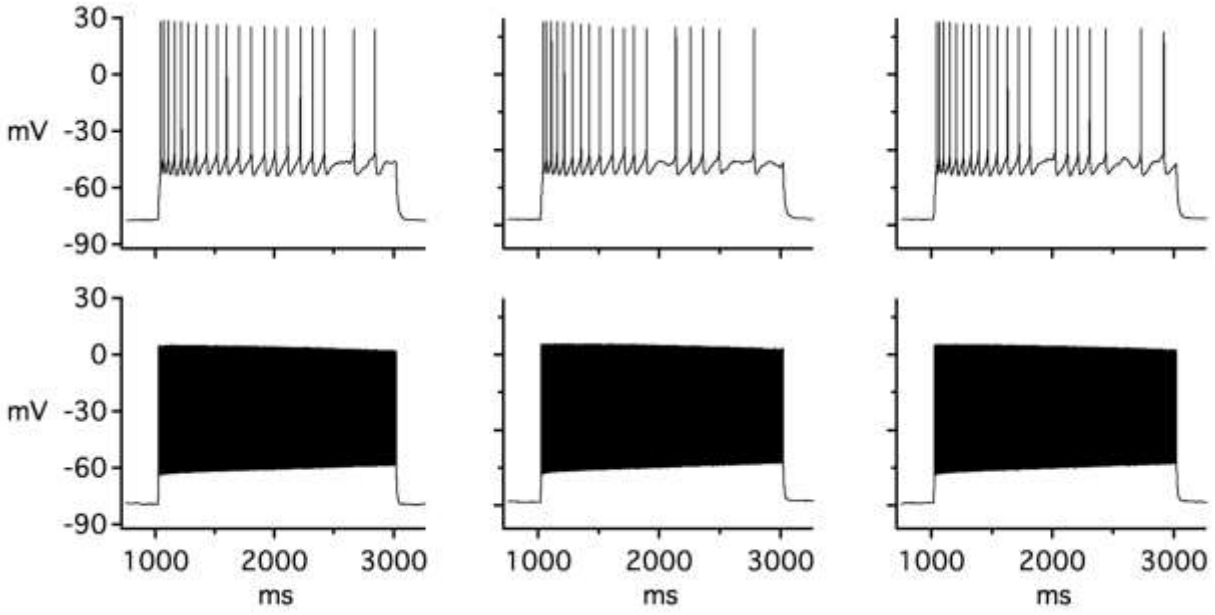

Figure 2. Experimental responses to current step protocol.
Responses to current steps starting at 1020 ms and lasting two seconds are shown. The protocol was repeated three times for each cell shown, and each column shows the response to a different repeat of the same stimulus protocol. Top: Recordings from a tdTomato+ Rorb-Cre cell. The current step amplitude was 270 pA. Bottom: Recordings from a tdTomato+ Pvalb-Cre cell. The current step amplitude was 340 pA.

Table 1. Electrophysiological features used in the model optimization procedure.

Feature Name	Feature Name
1. Firing frequency (Hz) (*average during stimulus*)	7. Resting potential (mV)
2. Action potential peak (mV)	8. Latency to first spike (ms)
3. Fast trough depth (mV)	9. Duration of first interspike interval (ms)
4. Slow trough depth (mV)	10. Coefficient of variation of interspike intervals
5. Time of slow trough as fraction of interspike interval	11. Adaptation index
6. Action potential width at half-height (ms)	12. Average interspike interval (ms)

MODEL CONFIGURATION

Morphology and Passive Properties

Models were optimized and run using NEURON 7.3 (Hines and Carnevale, 1997).

Morphologies in NEURON were generated by importing the SWC file for the target neuron (Morphology whitepaper in Documentation). In these reconstructions, the soma was represented as a sphere with a specified radius centered at the root node of the file. Since NEURON does not support spherical sections directly, NEURON's built-in Import3d function automatically converted this spherical somatic representation into a cylinder with the equivalent membrane area. It then connected child branches to the soma section with zero-resistance wires so that the child sections remain in the correct three-dimensional location while preserving the correct electrical connectivity.

Because the extent of axonal reconstruction varied considerably across cells, once the morphology was imported, any axonal segments present were removed, and a synthetic axon initial segment (AIS) 60 µm long with a 1 µm diameter was inserted instead. No additional axonal compartments were modeled.

The specific membrane capacitance (C_m) of the model and specific intracellular resistivity (R_a) were not free parameters during the main optimization procedure. However, when appropriate data were available, these parameter values were first estimated by using the PRAXIS method of NEURON's multiple run fitter to match the averaged, small, subthreshold responses to 0.5 ms step current injections of ±500 pA by varying the passive properties of a model using the reconstructed morphology of the cell (Major *et al*., 1994; Roth and Häusser, 2001). In this preliminary stage of the fitting process, no active conductances were used, and the voltage trace was fit directly without extracting features. The PRAXIS method varied C_m, R_a, and the specific membrane resistance (R_m) to best match the experimental data. These three values were assumed to be uniform across the entire cell. An example fit of this type is shown in **Figure 3**.

For aspiny neurons, the specific membrane capacitance was fixed to this value of C_m for the main optimization procedure. For spiny neurons (including sparsely spiny cells), it was assumed that the dendrites would have a higher effective specific membrane capacitance than the soma or axon due to the extra membrane area of spines (which were not explicitly modeled). Therefore, a specific membrane capacitance value for dendritic compartments was calculated using the estimate from the fitting procedure while assuming that the soma and axon had a specific membrane capacitance of 1 µF/cm^2.

The specific intracellular resistivity was also set to the value obtained from this fitting procedure. However, the specific membrane resistance value from this fit was not used directly since the leak conductance densities were free parameters during the main optimization procedure. If data for this fitting procedure were not available, standard values were used instead (100 Ω-cm for R_a, 1 µF/cm^2 for C_m of somatic and axonal compartments, as well as dendritic compartments of aspiny neurons, and 2 µF/cm^2 for C_m of dendritic compartments in spiny neurons).

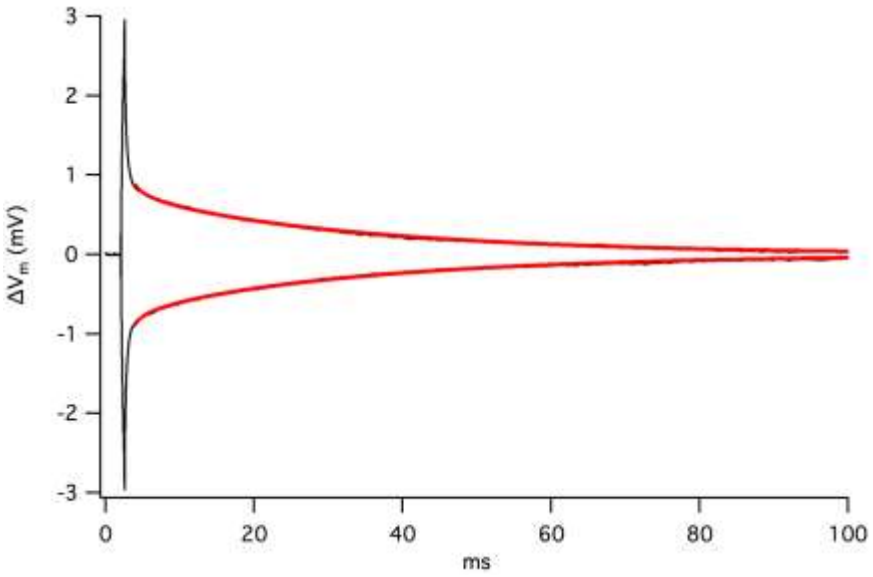

Figure 3. Fitting the specific membrane capacitance.
Black traces show the averaged experimental voltage deflection in response to a 0.5 ms, ±500 pA current step starting at 0 ms. Red traces show the model response after optimizing the specific membrane resistance, specific membrane capacitance, and specific intracellular resistivity for a uniform passive model based on the target cell's morphology. For this particular cell, the resulting C_m value was 2.56 µF/cm^2, and the R_a value was 121.95 Ω-cm.

Active Conductances

The next step in the fitting procedure was to introduce active conductances and tune their densities to optimize the response of a model to a step current injection (using electrophysiological features as described above). All active conductances were placed in the somatic compartment of the model. The dendritic compartments were passive for computational simplicity and because data from the somatic whole-cell recordings that would effectively constrain models with active dendrites were not available. Preliminary investigations were also made into optimizing models with active conductances in the axonal compartments as well, but with this approach significant difficulties were encountered in generating robust models in a computationally efficient manner, likely due to the increased number of parameters with those additional conductances. Therefore, in these models the active conductances in the somatic compartment can be considered to represent a perisomatic spiking zone (Hay *et al*., 2011).

The free parameters of the model that were adjusted during the optimization procedure were the densities of the active conductances (represented by "gbar," the maximum conductance density in a given compartment). An additional mechanism described intracellular Ca^{2+} dynamics using a first-order ODE that modeled the entry of Ca^{2+} due to the transmembrane current into a 100 nm sub-membrane shell with buffering/pumping; for this mechanism, the time constant of Ca^{2+} removal and the binding ratio of the Ca^{2+} buffer were also free parameters. A leak conductance was also inserted into all compartments of the model. The density of that leak conductance was a free parameter separately for each type of compartment—somatic, axonal, basal dendrite, and apical dendrite (when present)—and the reversal potential of the leak current was fixed to the experimentally measured resting membrane potential of the cell. The reversal potential of the I_h current was set to –45 mV (Kole *et al.,* 2006).

For most cells, a set of active conductances were employed based on those used by Hay *et al*. (2011) and which are listed in **Table 2**. Except for the free parameters described above, all other parameters of the active mechanisms were kept constant during the optimization. Most of these constant values matched those used by Hay *et al*. (2011), but the kinetic parameters of some of these conductances were adjusted to match more closely the original publications on which those models were based. The specific equations and parameters

were described in the provided ".mod" files that define each mechanism for the NEURON simulation environment. All these active conductances were modeled using a Hodgkin-Huxley formulation.

Using these original conductances, the optimized models matched experimental data rather closely for cells exhibiting wider action potentials (AP full width at half-height of 0.8 ms or more), which were typically spiny neurons, but it was difficult to fit neurons with narrow action potentials (AP full width at half-height of less than 0.8 ms), which in most cases were aspiny neurons. For cells with experimentally observed narrow action potentials, the best-fit models often produced action potentials with at least twice the target width, and this discrepancy in many cases became the major contributor to the overall error of those models.

Therefore, for these cells, a modified set of conductances were used instead (**Table 2**) based on additional studies from the literature. The fast and persistent sodium currents were replaced with an alternative kinetic model formulation based on the model of Carter *et al*. (2012). In this model, the rate of inactivation is not intrinsically voltage-dependent, but instead depends allosterically on the extent of channel activation; a separate ".mod" file defining this mechanism with a kinetic-style formulation was developed for this conductance ("NaV"). The slow inactivating potassium current was replaced by two other potassium current models: one representing a Kv1-like current (Foust *et al*., 2010) and another representing a Kv2-like current (Liu and Bean, 2014). Finally, the original M-current model was replaced by another ("*Im_v2*") from a model of rat CA1 pyramidal neurons (Vervaeke *et al*., 2006). With this revised set of conductances, the experimentally-measured AP widths in this set of cells were matched more closely by the optimized models.

In some cases, a spiny neuron exhibited narrower action potentials (under 0.8 ms), or an aspiny neuron exhibited wider action potentials (over 0.8 ms). In these cases, optimizations were performed with both sets of conductances, and the model that resulted in the better fit was selected.

In total, the models were optimized with 15 or 16 free parameters: 10 active conductance densities, 2 intracellular Ca^{2+} dynamics parameters, and 3 or 4 leak conductance densities (depending on the presence or absence of an apical dendrite).

Table 2. List of active conductances used in the biophysical models.

Conductances used for cells with wide APs	Conductances used for cells with narrow APs
Transient Na^+ conductance (*NaTs*)	Na^+ conductance (Markov-style formulation)
Persistent Na^+ (*Nap*)	
Hyperpolarization-activated cation conductance (*Ih*)	
High-voltage-activated Ca^{2+} conductance (*CaHVA*)	
Low-voltage-activated Ca^{2+} conductance (*CaLVA*)	
SK-type Ca^{2+}-activated K^+ conductance (*SK*)	
M-type (Kv7) K^+ conductance (*Im*)	M-type (Kv7) K^+ conductance, alternative (*Im_v2*)
Kv3-like K^+ conductance (*Kv3_1*)	
Fast inactivating (Kv4-like) K^+ conductance (*K_T*)	
Slow inactivating K^+ conductance (*K_P*)	Kv1-like K^+ conductance (*Kd*)
	Kv2-like K^+ conductance (*Kv2like*)

The names in parentheses refer to the specific ".mod" file that defines each conductance. Merged rows indicate conductances common to both fit types.

Simulation Conditions

Simulations were run in NEURON using the variable time step method. The equilibrium potentials of Na^+ and K^+ were set to values calculated from the internal and external solutions used in the *in vitro* experiments (E_{Na}

= +53 mV, E_K = –107 mV). The equilibrium potential of Ca^{2+} was calculated during each time step by NEURON using the Nernst equation using $[Ca^{2+}]_o$ = 2 mM and the value of $[Ca^{2+}]_i$ at that time (resting $[Ca^{2+}]_i$ was 100 nM). The temperature of the simulation also matched the temperature of the recording. All cells for which models were built were recorded at a temperature of near 34°C (Electrophysiology whitepaper in Documentation). For active conductances based on data recorded at temperatures differing from these conditions, the kinetics were scaled with a Q10 of 2.3 (Hay *et al*., 2011).

OPTIMIZATION PROCEDURE

Genetic Algorithm

The optimization procedure was based on that developed by Druckmann *et al*. (2007), using the code from Hay *et al*. (2011). A genetic algorithm procedure was used to iterate toward a set of 15–16 model parameters that matched the experimental data within a given tolerance. An "organism" for the genetic algorithm represented a given set of model parameters (conductance densities and calcium dynamics parameters). A population of 1,200 organisms was randomly generated, and during each generation a subset of organisms with high fitness (*i.e.* low total error function) was kept and bred together to produce a new set of organisms. Organisms also had a chance of undergoing random mutation. The procedure was executed for 500 generations and repeated independently for five different random seeds.

Including all features and parameters at once in this procedure often did not result in well-optimized models in the final generation. Therefore, a staged approach was used instead, in which the procedure was first run fitting only the first seven features listed in **Table 3**. Out of the runs with the five random seeds, the population containing the member with the lowest error was used as the starting population for a second stage of optimization. In the second stage, five additional runs with different seeds were carried out, now using the first seven as well as the next five features listed in **Table 3**. The model ("organism") with the lowest error function at the end of the procedure (after all stages) was kept as the representative model for that cell (**Figure 4**).

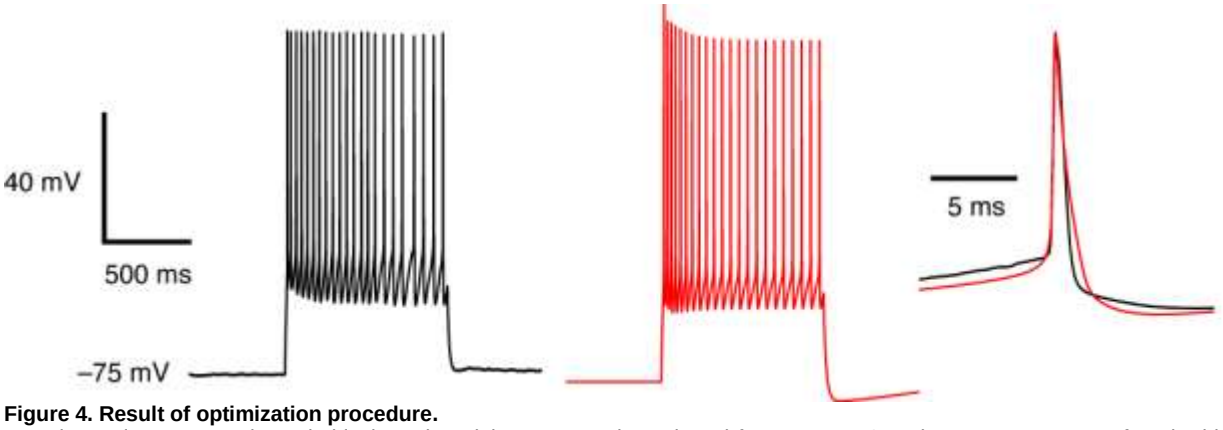

Figure 4. Result of optimization procedure.
Experimental traces are shown in black, and model traces are shown in red for an Nr5a1-Cre tdTomato+ neuron. *Left* and *middle* show the membrane potential in response to a constant current step for both the experiment and the optimized model. On the *right*, a close-up of individual spikes from the experiment and model is shown to facilitate comparison of the spike shapes.

Model Evaluation

The error function for a given feature was calculated as a modified "z-score", by taking the absolute value of the difference between the model's value of a feature and the average value from the different experimental repeats for the recorded cell, then dividing by the experimental standard deviation of the feature. The total error for the model was taken by averaging these individual feature errors; all 12 feature errors contributed equally to this combined measure. In some cases, the experimental variability of a given feature was extremely low, which effectively weighted a particular feature much more heavily than others. This caused issues with the algorithm's ability to find a solution that matched well across all features. Therefore, for each

feature a minimum level of tolerance that was deemed acceptable was determined (**Table 3**). When the experimental standard deviations were below these minimal variability levels, the latter were used in their place for optimization. This led to final models that were better balanced across all features used for the fitting procedure.

Table 3. Minimum tolerances of features used for fitting procedure and for metric calculation.

Feature Name	Tolerance
1. Firing frequency (spikes/sec)	0.5 spikes/sec
2. Action potential peak (mV)	2.0 mV
3. Fast trough depth (mV)	2.0 mV
4. Slow trough depth (mV)	2.0 mV
5. Time of slow trough as fraction of interspike interval	0.05
6. Action potential width at half-height (ms)	0.1 ms
7. Resting potential (mV)	2.0 mV
8. Latency to first spike (ms)	5.0 ms
9. Duration of first interspike interval (ms)	1.0 ms
10. Coefficient of variation of interspike intervals	0.01
11. Adaptation index	0.001
12. Average interspike interval (ms)	0.5 ms

In some cases, only a single sweep was available for a given stimulus duration and amplitude, so experimental variability could not be assessed. For these neurons, the minimum tolerance levels (**Table 3**) were used to evaluate the model fitness for all features. In some cases, this situation arose when only a single sweep in response to the longer, two-second square steps passed sweep-level quality control. In other cases, responses to the two-second square steps were available but exhibited a substantially different level of excitability than responses to the shorter, one-second steps recorded earlier in the experiment. If this was observed, a response to a one-second square step was selected for the optimization procedure so that the model would better reflect the initial electrical behavior of the recorded cell.

To facilitate model comparison, a metric for model fitting similar to the method described above, which was a "z-score" averaged across all features, was calculated and reported in the database. When calculating this metric, the predetermined minimum tolerances were always used so that the metric would be as consistent as possible across cells (regardless of the number of repeated sweeps available for optimization). In general, higher values of this metric indicated worse-fit models. However, since the same absolute tolerance levels were used across all cells, some models of neurons with high values of certain features (*e.g.* a higher than typical adaptation index) appeared worse by this metric even though the model features were proportionately closer to the experimental values. Users of these models ought to examine their performance on the aspects relevant to the particular experimental question rather than strictly relying on the provided metric to judge model performance.

MODEL GENERALIZATION

Once the models were fit, a "virtual experiment" was generated by applying all experimental protocols measured from the original cell to the model. The results of this "virtual experiment" were included in the database and presented on the web site, allowing for an assessment of how the model performs across a

wide variety of stimuli. Note that most of these stimuli were not used to train the model, so they can be used to establish how well the model generalizes across stimulus types (**Figure 5**).

For the noise stimulus protocols, a spike train metric that evaluates how closely the model compares to the spike timing variability present in the experiment was also calculated. This procedure is identical to the one used to evaluate the GLIF models (GLIF Models whitepaper in Documentation).

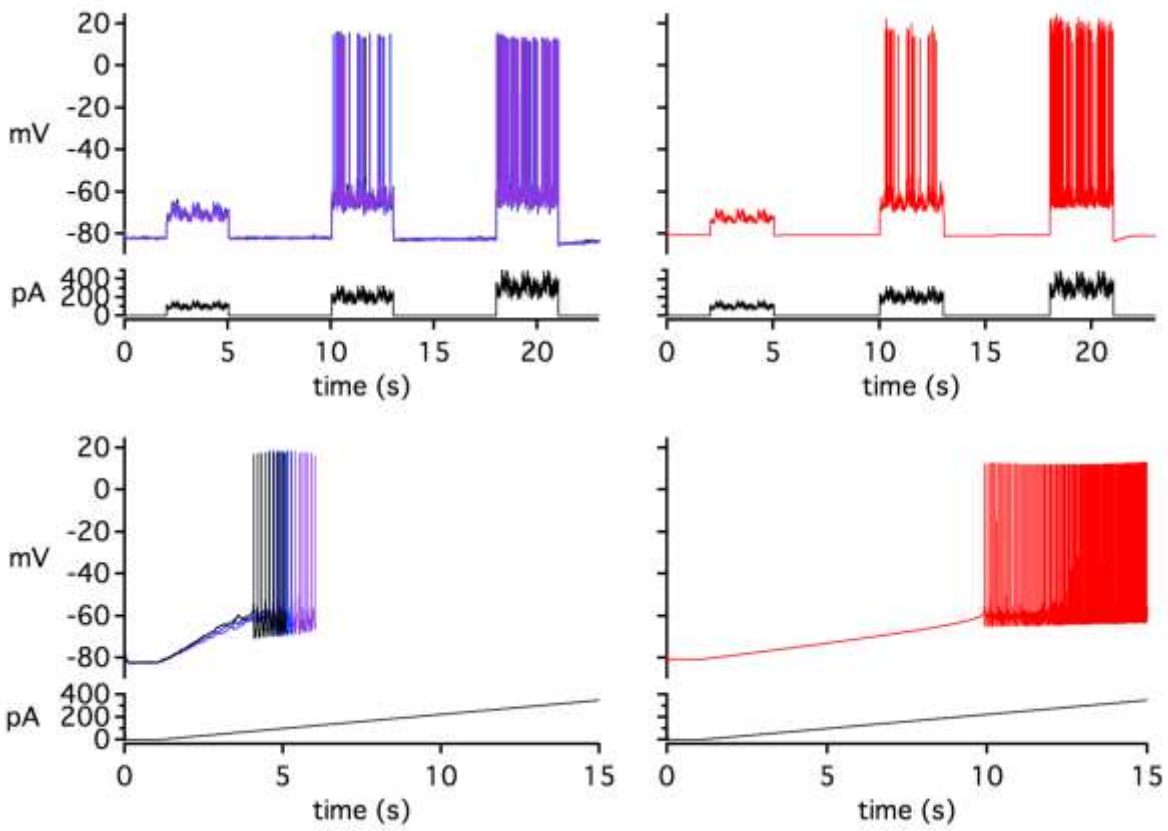

Figure 5. Model generalization to different stimulus types.
Experimental traces are shown on the left (different colors indicate different repeats of the same stimulus protocol). Model traces are shown on the right in red. The top graphs show the response of a Scnn1a-Tg3-Cre tdTomato+ cell and its corresponding model to a noisy current stimulus. The bottom graphs show the responses of the same cell to a slow current ramp stimulus. Experimental ramp responses do not cover the full interval because sweep acquisition was halted after several spikes were evoked to prevent overstimulation of the cell.

Limitations of the Models

Models generated from the described procedure and made available in the database typically could reproduce the original data used in the optimization with a high degree of accuracy. In many cases, these models could generate responses to other stimuli that closely resembled the experimental data as well.

However, certain limitations of models were observed in multiple cases, where responses to a subset of stimuli diverged significantly from what was observed in the experiment. This could be due to aspects of the modeling approach – such as the use of the identical, canonical set of “generic” conductances across all models (rather than customizing the properties or combinations of conductances based on other information about the targeted cells), or the absence of certain features in the optimization procedure that would select for models with improved robustness to particular circumstances.

Failures to repolarize at high stimulus intensities
A subset of models exhibited behavior in which they failed to repolarize completely when stimulated at high intensity (typically in response to high-amplitude square step stimuli or noise stimuli), and instead would lock up at a moderate potential, unable to fire additional action potentials. In some cases, the model would not repolarize even after the stimulus ended. However, these models often performed fairly well at lower stimulus intensities (and correspondingly lower firing rates).

Shallow activation curves for fast-spiking neurons
Most of the models of fast-spiking aspiny neurons (typically tdTomato+ neurons from the Pvalb-Cre line cross) could not fully reproduce the sharp slope of the experimental F-I curves (firing frequency versus stimulus intensity) measured from these cells, which could often increase by 40 spikes/sec or more with a 20 pA change in stimulus intensity. Instead, the models started to fire at lower stimulus intensities than observed experimentally and more gradually increased their firing rate with increasing stimulus intensity.

Difficulty in reproducing highly transient responses
Some neurons produced a very transient response to square current steps, in which they fired a few action potentials early in the step and then remained silent for the rest of the stimulus period (or fired an occasional spike late in the stimulus period). The models produced for these cells often were unable to match this transient behavior fully, especially across a range of stimulus intensities. In some cases, they would produce a similar response to that used for the optimization procedure, but would then produce a more sustained response at higher stimulus levels that was not observed experimentally. In other cases, the model would produce a response that was transient, but lasted longer than observed in the experiment. This may have been due to limitations of the set of conductances used in these models or failure to include relevant features that would optimize for this transient behavior.

Excessive hyperpolarization in response to negative current steps
Models were only optimized with suprathreshold responses to positive-going current steps, and most of the active conductances in the model open only in response to depolarization. Therefore, the models do not reproduce the rectification of responses to hyperpolarizing current steps that were frequently observed experimentally (which may have been due to mechanisms like inwardly-rectifying potassium channels). Because of this, the hyperpolarizing deflections to negative current steps were often larger than those observed experimentally. This limitation may be less of a factor in many potential uses of these models, as the hyperpolarized potentials at which these effects occur are less likely to be encountered with simulated physiological synaptic activity (versus the effects of current injection via a simulated whole-cell electrode).

Again, users ought to examine the performance of individual models with various types and amplitudes of stimuli and choose the models that would be most appropriate (based on their performance) for the particular intended study.

REFERENCES

Carter BC, Giessel AJ, Sabatini BL, Bean BP (2012) Transient sodium current at subthreshold voltages: activation by EPSP waveforms. *Neuron* 75:1081–1093.

Druckmann S, Banitt Y, Gidon A, Schürmann F, Markram H, Segev I (2007) A novel multiple objective optimization framework for constraining conductance-based neuron models by experimental data. *Frontiers in Neuroscience* 1:7–18.

Druckmann S, Berger TK, Schürmann F, Hill S, Markram H, Segev I (2011) Effective stimuli for constructing reliable neuron models. *PLoS Computational Biology* 7:e1002133.

Foust AJ, Yu Y, Popovic M, Zecevic D, McCormick DA (2011) Somatic membrane potential and Kv1 channels control spike repolarization in cortical axon collaterals and presynaptic boutons. *Journal of Neuroscience* 31:15490-15498.

Hay E, Hill S, Schürmann F, Markram H, Segev I (2011) Models of neocortical layer 5b pyramidal cells capturing a wide range of dendritic and perisomatic active properties. *PLoS Computational Biology* 7:e1002107.

Hines ML, Carnevale NT (1997) The NEURON simulation environment. *Neural Computation* 9:1179–1209.

Kole MH, Hallermann S, Stuart GJ (2006) Single I_h channels in pyramidal neuron dendrites: properties, distribution, and impact on action potential output. *Journal of Neuroscience* 26:1677–1687.

Liu PW, Bean BP (2014) Kv2 channel regulation of action potential repolarization and firing patterns in superior cervical ganglion neurons and hippocampal CA1 pyramidal neurons. *Journal of Neuroscience* 34:4991–5002.

Major G, Larkman AU, Jonas P, Sakmann B, Jack JJ (1994) Detailed passive cable models of whole-cell recorded CA3 pyramidal neurons in rat hippocampal slices. *Journal of Neuroscience* 14:4613–4638.

Roth A1, Häusser M (2001) Compartmental models of rat cerebellar Purkinje cells based on simultaneous somatic and dendritic patch-clamp recordings. *Journal of Physiology* 535:445–472.

Vervaeke K, Hu H, Graham LJ, Storm JF (2006) Contrasting effects of the persistent Na+ current on neuronal excitability and spike timing. *Neuron* 49:257–270.